

Catalytic Partial Oxidation of Methane to Methanol Using Nitrous Oxide

Akanksha Tyagi

A Dissertation Submitted to
Indian Institute of Technology Hyderabad
In Partial Fulfillment of the Requirements for
The Degree of Master of Science



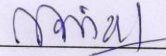
भारतीय प्रौद्योगिकी संस्थान हैदराबाद
Indian Institute of Technology Hyderabad

Department of Chemistry

April, 2014

Declaration

I declare that this written submission represents my ideas in my own words, and where others' ideas or words have been included, I have adequately cited and referenced the original sources. I also declare that I have adhered to all principles of academic honesty and integrity and have not misrepresented or fabricated or falsified any idea/data/fact/source in my submission. I understand that any violation of the above will be a cause for disciplinary action by the Institute and can also evoke penal action from the sources that have thus not been properly cited, or from whom proper permission has not been taken when needed.



(Signature)

Akanksha Tyagi

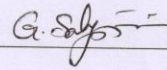
cy12m1002

Approval Sheet


This thesis entitled **Catalytic Partial Oxidation of Methane by Nitrous Oxide** by Akanksha Tyagi is approved for the degree of Master of Science from IIT Hyderabad.



(Examiner)



Examiner



(Adviser)

(Chairman)

Acknowledgements

It is my immense pleasure to express my gratitude to Dr. Ch. Subrahmanyam for his constant inputs and encouragement that helped me to complete this project successfully. I would also like to thank Department of Chemistry, IIT Hyderabad for providing me financial support.

This journey would not have been so smooth and informative without the healthy lab environment provided by my lab mates. I extend my sincere thanks to Mrs. Shaik Mahammadunnisa and other research scholars for helping me out throughout the project.

Above all I would like to thank god and my parents for their unconditional support. Without them I would not have been a fraction of what I am today.

Akanksha Tyagi

Dedicated to

My Parents

And

Sister

Abstract

Partial oxidation of methane to methanol using nitrous oxide is an important reaction which has the potential of curbing the twin problems of energy and environment. Both the reactants are major greenhouse gases and they can be made to react together to yield a product which holds the potential to replace the existing non-renewable energy sources: coal and petroleum. Partial oxidation of methane is usually done using steam reforming process. But because practical limitations, this method is not used on industrial scale. Hence the focus has shifted to find new ways like thermal and plasma catalysis which could bring down the involved cost and make the process free for general use. Lot of work has been reported on partial oxidation of methane using N_2O using thermal catalysis. But most of them involve the use of expensive metals like Rh, Ru, Pt, Au etc.

This work was aimed to design an economical and novel catalyst which can carry out the concerned reaction at low temperatures. We first prepared a series of cobalt oxide doped with cerium oxide catalysts which were tested for decomposition of nitrous oxide and then the best one among them was subjected to partial oxidation of methane. All the catalysts were characterized using physic-chemical techniques like XRD, Raman spectroscopy, UV-Vis spectroscopy, BET analysis and TPR. Also the best were analyzed using TEM and XPS too. A pictorial representation of the work is shown in figure 1.

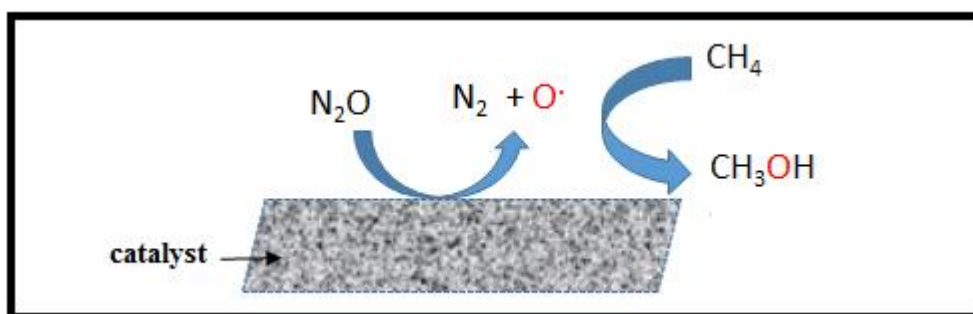


Figure 1: Pictorial representation of partial oxidation of methane to methanol

Nomenclature

Abbreviations

1. P-XRD: Powder X-ray Diffraction
2. UV: Ultraviolet
3. BET: Brunner Emmett Teller
4. TPR: Temperature Programmed Reduction
5. TEM: Transmission Electron Microscope
6. TPD: Temperature Programmed Desorption
7. TCD: Thermal Conductivity Detector
8. CCD: Charged Coupled Detector
9. SHS: Self propagating High temperature Synthesis
10. LCS: Low temperature Combustion Synthesis
11. SCS: Solution Combustion Synthesis
12. FS: Flame Synthesis
13. GS: Gel combustion Synthesis
14. SGC: Sol Gel Combustion
15. EC: Emulsion Combustion
16. VC: Volume Combustion
17. HREM: High Resolution Electron Microscopy
18. XPS: X-ray Photoelectron Spectroscopy
19. ESCA: Electron Spectroscopy for Chemical Analysis
20. GC-MS: Gas Chromatography Mass Spectrometer
21. GC-TCD: Gas Chromatography Thermal Conductivity Detector
22. FCC: Face Centered Cubic
23. LMCT: Ligand to Metal Charge Transfer
24. MFC: Mass Flow Controller
25. TWC: Three Way Catalysis
26. ZSM: Zeolite Socony Mobil

Symbols

1. α : Alpha
2. β : Beta
3. ϕ : Phi: Fuel: Oxidant ratio
4. ϕ_0 : Work function
5. λ : Wavelength

6. θ : Theta
7. ν : Frequency
8. h : Planck constant
9. N_A : Avogadro constant
10. E_a : Activation Energy
11. \AA : Angstrom
12. μm : Micrometer
13. nm : Nanometer
14. mm : Millimeter
15. ml : Milliliter

Contents

List of figures	12
List of tables	12
1. Chapter 1: Introduction	13
1.1 Catalytic decomposition of N ₂ O	13
1.2 Partial oxidation of methane	15
2. Chapter 2: Experimental section	17
2.1 Catalyst preparation methods	17
2.1.1. Hydrothermal synthesis	17
2.1.2. Coprecipitation synthesis	17
2.1.3. Combustion synthesis	18
2.2 Characterization techniques	19
2.2.1. X-ray diffraction for powder catalysts	19
2.2.2 Surface area determination: BET Analysis	20
2.2.3 Temperature Programmed Reduction	21
2.2.4 Raman Spectroscopy	21
2.2.5 Transmission Electron Microscopy (TEM)	22
2.2.6 X-ray Photoelectron Spectroscopy (XPS)	22
3. Chapter 3: Decomposition of nitrous oxide	24
3.1 Introduction	24
3.2 Experimental section	24
3.2.1 Preparation of Co ₃ O ₄	24
3.2.1.1. Combustion synthesis:	24
3.2.1.2. Hydrothermal synthesis	25
3.2.1.3. Coprecipitation synthesis	25

3.2.2. Preparation of Ce/Co catalysts using SCS	25
3.3 Results and discussion	25
3.3.1 Characterization and activity measurements of Co_3O_4	26
3.3.1.1 P-XRD	26
3.3.1.2 Surface area determination	27
3.3.1.3. Raman Spectroscopy	27
3.3.1.4. UV Visible Spectroscopy	28
3.3.1.5. Temperature Programmed Reduction (TPR)	29
3.3.1.6. Activity measurement of Co_3O_4	29
3.3.2 Characterization and activity measurements of (xCeCo) catalysts	31
3.3.2.1 P-XRD	31
3.3.2.2 Determination of surface area (BET analysis)	33
3.3.2.3 TEM	33
3.3.2.4 XPS	34
3.3.2.5. Raman spectroscopy	34
3.3.2.6. UV-Visible spectroscopy	35
3.3.2.7. TPR	36
3.3.2.8. Activity measurement:	37
3.4 Conclusions	38
4. Chapter 4: Partial oxidation of methane using nitrous oxide	40
4.1 Introduction	40
4.2 Experimental section	40
4.2.1 Catalyst preparation:	40
4.2.2 Catalyst characterization	40
4.2.3. Activity measurements	41
4.3 Results and discussions	41

4.4 Conclusions	42
5. References	44

List of figures

Figure 1: Pictorial representation of partial oxidation of methane to methanol	6
Figure 2: Emission of X-rays	19
Figure 3: Electronic levels in an atom	23
Figure 4: A sample prepared using combustion synthesis	25
Figure 5: Activity measurement experimental setup	26
Figure 6: P-XRD patterns of Co_3O_4 prepared by different methods	27
Figure 7: Raman spectra of Co_3O_4	28
Figure 8: UV-Vis. Spectra of Co_3O_4	28
Figure 9: TPR of Co_3O_4	29
Figure 10: Decomposition of nitrous oxide by Co_3O_4	30
Figure 11: XRD pattern of xCeCo catalysts	32
Figure 12: TEM image of (a) CeO_2 and (b) 10CeCo catalyst	33
Figure 13: Core level XPS spectra of 10CeCo (a): Co (2p), (b): Ce (3d)	34
Figure 14: Raman spectra of xCeCo catalysts	35
Figure 15: UV-Visible spectra of xCeCo catalysts	35
Figure 16: TPR profile of xCeCo catalysts	36
Figure 17: N_2O decomposition by xCeCo	37
Figure 18: Activation energy calculations for Co_3O_4 , 10CeCo and 20CeCo	38
Figure 19: Conversion data for N_2O and CH_4	41
Figure 20: Selectivity profile of various products	42

List of tables

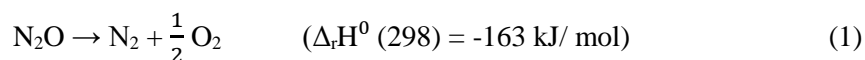
Table 1: BET surface area of Co_3O_4 catalysts	27
Table 2: lattice parameters, surface area and particle diameter of xCeCo catalysts	32
Table 3: Selectivity towards different products upon partial oxidation of CH_4 using N_2O	43

1. Chapter 1

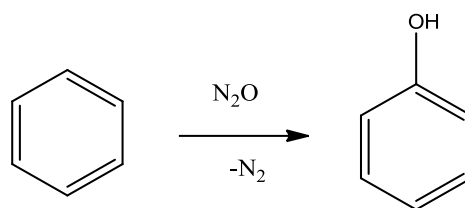
Introduction

1.1 Catalytic decomposition of N₂O

Recent studies have proved N₂O to be one of the most dominant ozone-depleting substance [1]. Also with a global warming potential, nearly 300 times more than CO₂ and a lifetime of nearly 100 years, N₂O is a potential threat to atmosphere [2]. About 40% of total global N₂O emissions are a result of human activities like agriculture, transportation, combustion of fossil fuels and industries involved in preparation of adipic and nitric acid. Many natural processes, like nitrogen cycle and breakdown of nitrogen by bacteria in soil and oceans too are responsible for nitrous oxide emissions. It is also released as a by-product during the abatement of other environmentally harmful species like three-way catalytic decomposition of NO_x, CO, hydrocarbons etc. [3]. Hence the growing levels of N₂O in atmosphere is of major concern. To curb this many new ways of emission reduction are being investigated. Broadly there can be two possible ways, either controlling the amount of N₂O being released or by decomposition of released N₂O. Later turns out to be more realistic as lot of time needed to bring down the current emission levels. Although thermodynamically unstable, the N₂O molecule is quiet stable room temperature. In the asymmetric N-N-O molecule the N-N bond order is about 2.7 and that of N-O about 1.6. Hence it is this N-O bond which may be cleaved during decomposition of N₂O as per equation 1.



The decomposition reaction is useful in many applications like use of nitrous oxide as an anesthetic, reprocessing of fossil fuel rods using nitric acid to name few [2]. One of the most famous example of usage of N₂O decomposition is in hydroxylation of benzene using Fe ZSM-5 [4]



This reaction is an industrial procedure for preparation of phenol. Phenol is used in synthesis of chemicals like caprolactam and adipic acid.

Various attempts have been reported on the catalytic decomposition of N_2O . Initially pure metals like Pt [3] and Au [5] were employed as catalysts. They were effective but needed high operational temperatures. Also they were easily deactivated by the products of reaction (N_2 and O_2) when used for a longer time. This along with their high cost forced researchers to look out for other alternatives. It was realized that the efficiency of the catalyst could be enhanced by using it with a proper support. M. Hussain et al. used Rh supported on mesoporous silica (SBA-15-S) as catalyst [6]. H. Yoshida et al. studied the effect of the nature of support on the catalytic activity of Pd and Pt for N_2O decomposition [7]. Metal oxides, both pure and mixed have also been employed for this reaction. H. Zhou et al. used Copper and cerium oxide mixed oxide as catalyst [8]. While pure CeO_2 was inactive, CeO_2 doped CuO showed better activity than CuO for N_2O decomposition.

Cobalt oxides, especially those with a promoter, have been shown to exhibit good catalytic properties in many processes like oxidation of CO [9, 10], CH_4 [11], higher hydrocarbons and ammonia as well as reduction of nitrous oxide [12]. E. Wilczkowska et al. demonstrated the use of pure cobalt oxide spinel (Co_3O_4) for N_2O decomposition [13]. Co_3O_4 has cubic structure and is expected to have 1:2 ratio of Co^{+3} : Co^{+2} ions. However presence of non-stoichiometry results in an increased concentration of oxide ions which in turn causes an increased ratio of Co^{+3} due to charge transfer to oxygen. The redox couple of Co^{+3}/Co^{+2} plays an important role in the usage of cobalt oxide as catalyst. But undoped cobalt oxide has numerous limitations for its use as catalyst for N_2O decomposition especially at higher temperatures because of reduction of its active phase to CoO. Further the catalyst particles tend to sinter and form clusters which results in reduced activity. Hence a dopant is needed which apart from stabilizing the catalyst, provides additional and enhanced catalytic activity too. Dou Zhe et al. used gold doped Co_3O_4 and Zn- Co_2O_4 catalysts [14]. They found that although Zn Co_2O_4 was more active than Co_3O_4 , gold doping increased activity of Co_3O_4 more than Zn/ Co_2O_4 . Among the various structural modifiers available, cerium oxide (CeO_2) seems a good candidate because of its well-known 'oxygen storage capacity'. Cerium oxide plays an important role in two most important industrial processes: three way catalysis (TWC) and fluid catalytic

cracking. Apart from this cerium oxide has been used in the treatment of gaseous emissions like SO_x , and liquid wastes. However in all these processes it always acts as structural/electronic promoter or as co-catalyst but never as true catalyst. Hence, effective stabilization of the dispersed state of transition metal oxides by prevention of sintering, retention of their high surface area and its redox/oxidation properties along with high oxygen mobility further encourage usage of cerium oxide in preparation of efficient transition metal oxide based catalysts.

1.2 Partial oxidation of methane

One of the recent use of decomposition of nitrous oxide is in the partial oxidation of methane to methanol. Methane (CH_4) is a potential greenhouse gas. Its' global warming potential over a 100 year time scale is nearly 25 times that of carbon dioxide (CO_2) [2]. Also methane is the major constituent of natural gas (95%) and hence it is potential clean source of energy too. The natural reserves of methane are comparable to that of petroleum. But they are located in remote places and so in order to use methane as fuel, it needs to be transported from these reserves to centers of consumption. It is not an easy task since the boiling point of methane is -165°C and requires expensive liquid nitrogen refrigeration throughout the transportation. Hence it is uneconomical to bring methane to market in the gaseous form. The most attractive alternative is to convert methane to any other liquid product which would overcome these limitations and at the same time retains its energy content. Methanol (CH_3OH) is one such product. And hence partial oxidation of methane to methanol is an extensively studied area.

Methanol is one of the most important industrial chemicals and its major application is its use as solvent or an as intermediate for many chemicals that are used as fuels or fuel additives. When blended with gasoline, methanol can used directly as an automobile fuel. Natural gas can be converted to products like methanol, formaldehyde etc. via two ways: direct and indirect. Indirect routes involve conversion of methane to carbon monoxide and hydrogen (a mixture called syngas) by steam reforming followed by catalytic conversion of syngas to methanol. On the other hand direct routes as the name suggests involve use of an oxidizing agent which oxidizes methane to methanol [15]. Commercially this is done by indirect route. But this is not a profitable process since steam reforming of methane is an energy intensive process which requires high operational temperatures and pressure which increases the cost of production. In order to reduce the reforming cost, direct routes have been developed. Here also one limitation being faced is that although formation of methanol is thermodynamically favored but formation of oxides of carbon like carbon monoxide and dioxide is even more

favorable and hence it becomes necessary that the oxidation is controlled so as to give only methanol.

Initial catalytic reactions for methane oxidation were based on the concept of activation of C-H bond. Of the most commonly used catalysts were molybdenum and vanadium based. First report of usage of molybdenum oxide, MoO_3 was published by Dowden and Walker [16]. Later Spencer exploited silica supported MoO_3 catalysts [17]. However soon it was realized that this is not a viable process and hence a new concept was developed. This involved a catalyst capable of transferring and stabilizing active oxidizing species. Some of the early works involved use of mixed metal oxides like Mo-V-Cr-Bi-Ox/ SiO_2 [18]. Since this process is an oxidation process, several oxidizing agents have been tested like air [19], peroxide [20] etc. Nitrous oxide too has been exploited for the said reaction. One of the earliest report for this was by Lunsford and co-workers who used Mo/ SiO_2 [21]. Later other catalysts like Ru/alumina [22], Co-Al/Au [23] etc. were also tested.

Earlier Xue et al. have reported decomposition of nitrous oxide over cerium oxide promoted cobalt oxide catalyst prepared by Coprecipitation method [24]. However it is well known that catalyst activity can be modified by the preparatory methods [25]. This is true for Co_3O_4 . Hence we first prepared pure Co_3O_4 using different preparation methods: combustion, Coprecipitation and hydrothermal and tested their activity for N_2O decomposition. Later the best one was chosen and was doped with varying contents of cerium oxide (CeO_2) as to get a series of CeO_2 doped Co_3O_4 catalysts. All were further subjected for N_2O decomposition. The one which was showing best activity for nitrous oxide decomposition was then tested for methane oxidation.

2. Chapter 2

Experimental section

2.1 Catalyst preparation methods

The catalysts used in the project were prepared by three different methods. A brief description of all three is given below.

2.1.1. Hydrothermal synthesis: Hydrothermal synthesis can be defined as a method of synthesis of materials that depends on the solubility of minerals in hot water under high pressure. The crystal growth is performed in an apparatus consisting of a steel pressure vessel called an autoclave, in which a nutrient is supplied along with water. A temperature gradient is maintained between the opposite ends of the growth chamber. At the hotter end the nutrient solute dissolves, while at the cooler end it is deposited on a seed crystal, growing the desired crystal. Possible advantages of the hydrothermal method over other types of crystal growth include the ability to create crystalline phases which are not stable at the melting point. Also, materials which have a high vapor pressure near their melting points can also be grown by the hydrothermal method. The method is also particularly suitable for the growth of large good-quality crystals while maintaining good control over their composition. Disadvantages of the method include the need of expensive autoclaves, and the impossibility of observing the crystal as it grows.

2.1.2. Coprecipitation synthesis: Coprecipitation means the precipitation of one substance along with another. Sometimes the concentration of a particular substance in the solution is so low that it can't be precipitated in the usual way. Coprecipitation of a salt happens in such a case. This method involves the utilization of the concept of solubility and ionic product. The reactants are dissolved in water and then an appropriate precipitating agent is added to it. When the ionic product of a substance (salt) exceeds its solubility product, the salt precipitates out of the solution. The synthesis involves nucleation, growth and digestion. Also the choice and amount of precipitating agent added is important in ensuring complete precipitation. Generally slow and small addition of the precipitating agent is important for complete precipitation.

2.1.3. Combustion synthesis: Combustion synthesis stands out an important and popular method which enables ample control over the resultant shape and size of the synthesized solids. Combustion synthesis means synthesis of compounds in a wave of chemical reaction (combustion) that propagates over a starting reaction mixture owing to layer by layer heat transfer. It is an exothermic redox process. The term combustion covers flaming, smoldering as well as explosive reactions. Also depending on the nature of reactants and the exothermicity of reaction combustion synthesis is classified as: self-propagating high temperature synthesis (SHS), low temperature combustion synthesis (LCS), solution combustion synthesis (SCS), flame synthesis (FS), gel combustion (GS), sol gel combustion (SGC), emulsion combustion (EC) and volume combustion (VC).

Solution combustion synthesis: The process involves an aqueous solution of a combustible redox mixture (metal precursors) and a fuel. Solution is heated to a particular temperature called ignition temperature (T_i), the point at which the combustion synthesis reaction is dynamically activated without further external heat supply. The actual combustion temperature, T_c is the maximum temperature achieved and this can be as high as 1500°C . The process duration is around 10 seconds. Some advantages of SCS are: tight control over reaction stoichiometry and homogeneity of products because of solution synthesis, high purity products: high temperature volatilizes impurities, fast process and no special equipment is needed, rapidity of the process allows the formation of metastable phases too.

Various metal precursors are nitrates, carboxylates, hydrazine, hydrazide, hydrazinium etc. All of them have an underlying requirement that they are a combination of redox couple and upon decomposition, they should give gaseous products like CO_2 , H_2O , N_2 and fine oxide particles of small size and high surface area. Also they should have good aqueous solubility since this ensures concentrated solutions. Fuel is an organic compound which is a source of carbon and hydrogen and which on combustion releases CO_2 , H_2O and heat. Also it should be able to form complexes with metal ions facilitating homogenous mixing of cations in solution. Commonly used fuels are glycine, urea, hydrazine or a precursor containing a carboxylate anion like citric acid. The products' morphology can be controlled by modifying the reactants stoichiometry which is governed by a ratio called oxidant-fuel ratio, ϕ . As amount of fuel increases, the heat realized also increases which increases gas phase production which gives particles of small size and spongy morphology. For better intimacy throughout the reaction mixture, stoichiometry is essential. The farther from this ratio, the longer the time needed for ignition to occur. This happens in fuel rich and fuel lean conditions. However the delay is more for later. In fuel lean condition, delay is because of less fuel is

dispersed in larger oxidizer mass. Whereas mass transfer control of external oxygen needed for complete combustion of fuel is the reason for delay in fuel rich condition. Hence an optimum ratio as per requirement is needed for desired results [26].

2.2 Characterization techniques

All the catalysts that were used, were characterized using the techniques discussed below.

2.2.1. X-ray diffraction for powder catalysts

Most catalysts are crystalline solids and hence X-ray powder diffraction (XRD) is becoming a fundamental technique enabling us to evaluate nature of crystalline phases, their concentration in the solid and crystallite size. X-rays are generated as a result of bombardment of a metal electrode by high energy electrons accelerated by a large potential, as shown in fig.2.

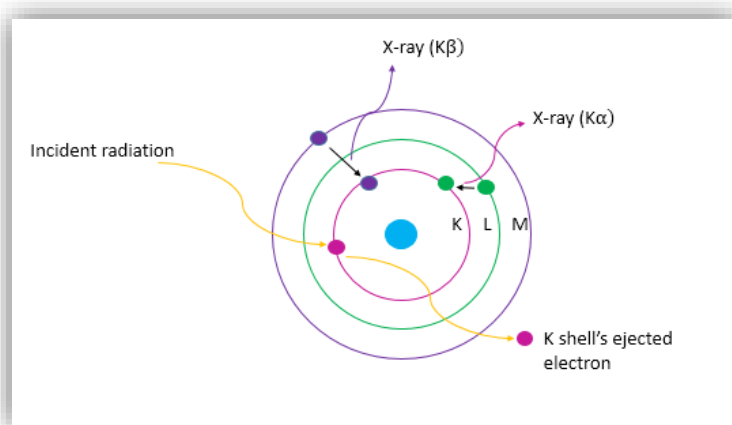


Figure 2: Emission of X-rays

The incident electrons result in emission of electrons from the inner shell (K) of metal. This creates a vacancy in the atom. Now if another electron from L level comes down to fill this vacancy some radiation is released which is called K α radiation. On the other hand if an electron from M shell fills the vacancy the radiation released is called K β . These two radiations are characteristic of the metal used. However since the K α is more intense than K β , it is used in the experiment.

When X-rays interact with matter, they are diffracted and scattered by the electrons present in the atom. And in a crystal, the patterns are seen as a result of an array of all such atoms. XRD patterns are a plot between intensity and angle, 2θ . The spacing between planes in a crystal can be calculated by Bragg's law

$$n\lambda = 2d \sin \theta$$

Here, λ is the wavelength of X-ray source. n is the order of diffraction. d is inter planar spacing and Θ is angle of diffraction. Also the particle size can be determined by Scherrer's formula

$$\langle L \rangle = \frac{B \cos(\frac{2\theta}{2})}{\lambda k}$$

Where L is particle size, B is the broadening of signal, k is the constant which is usually taken to be 1.

In project, XRD was used to investigate the bulk phases present in the sample and to determine the calcination induced solid-solid phase transformation, if any. This was done using PANalytical X'pert pro X-ray diffractometer with Cu K_{α} ($\lambda = 1.541 \text{ \AA}$ radiation, 30 mA, 40 kV).

2.2.2 Surface area determination: BET Analysis

Specific surface area of a powdered solid is obtained by physical adsorption of gas on the surface of the solid and by calculating the amount of adsorbate gas corresponding to a monomolecular layer on the surface. Brunner Emmett Teller method is one of the most reliable and widely used methods of surface area determination. It can be thought as a generalization of Langmuir adsorption isotherm. This theory explains multilayer adsorption, however all the postulates of Langmuir isotherm are applicable to every monolayer adsorption. BET equation is:

$$\frac{p}{(p_0 - p)V_{total}} = \frac{1}{C V_{mono}} + \frac{(C - 1)p}{C V_{mono} p_0}$$

Where

V_{mono} : Volume of the gas required to form one complete monolayer of adsorbate on the surface of the adsorbent.

V_{total} : Total volume of gas adsorbed, on the surface of the adsorbent, at the given temperature and pressure reduced to standard condition.

p_0 : Saturated vapor pressure of the gas at temperature T and p is the pressure of the gas.

C : constant, at given conditions, which depends on the nature of the gas for a particular adsorbate- adsorbent pair. $C = e^{((E_1 - E_L)/RT)}$

Where E_1 is heat of adsorption in the first layer and E_L is that in second and higher layers and is equal to the enthalpy of liquefaction. It is an indication of the magnitude of the adsorbent/adsorbate interactions.

A plot between $\frac{p}{(p_0 - p)V_{total}}$ (y axis) and $\frac{p}{p_0}$ (x axis) gives $\frac{1}{C V_{mono}}$ as intercept and $\frac{(C - 1)}{C V_{mono}}$ as slope. V_{mono} is used to calculate the surface area of adsorbate.

The experiment is performed at 77K and the measured parameter is pressure p , amount of added gas V_{total} is controlled by the instrument. V_{mono} and C are calculated by the computer and are used to calculate surface area as per the equation

$$\text{Specific surface area} \left(\frac{m^2}{g} \right) = \frac{A_m N_A V_{mono}}{W V_0}$$

Here N_A is Avogadro constant = 6.023×10^{23}

A_m is the cross sectional area of the adsorbate molecule (for N_2 it is $.162 \text{ nm}^2$ at 77K)

W is the weight of the sample and $V_0 = 22.4 \text{ L mol}^{-1}$.

In the present work, the BET surfaces were determined by N_2 adsorption using a Quantachrome autosorb automated gas sorption analyzer (NOVA 2200e). Before keeping samples for analysis, they were oven dried at 300°C for 12 hrs under vacuum and flushed with Argon gas for 2 hrs. All the BET values in this study were within $\pm 5\%$ error. N_2 physisorption was used to measure the surface area. The principle is physisorbed N_2 forms a monolayer over the adsorbent at low temperatures. This monolayer is independent of the size of the adsorbent molecules and depends only on the nature of adsorbed gas's molecules. Hence knowing the size of gas molecule, one can calculate the whole surface area of the adsorbent.

2.2.3 Temperature Programmed Reduction

Temperature Programmed Reduction (TPR), temperature programmed decomposition (TPD) and catalytic activity measurements were carried out in a flow system (Quantachrome autosorb-IQ automated gas sorption Analyzer) equipped with a thermal conductivity detector (TPR-TCD). For TPR measurements, 50mg of the sample was sandwiched between quartz wool plugs in a U-shaped quartz reactor and flushed with He for 30 min. The TPR profiles were obtained by heating the sample from room temperature to the desired temperature (600°C) in 10% H_2 in Ar, (gas flow rates 40 ml min^{-1} and heating rate of $10^\circ\text{C min}^{-1}$) and the gaseous products were sampled through a fine control leak valve to TCD after passing through a cold trap to remove H_2O . Quantitative analysis was done by integrating the reduction signal and comparison was made by pre-calibrated signals.

2.2.4 Raman Spectroscopy

Raman scattering is the inelastic scattering of light with momentum and energy transfer between the photons and scattering material. It is one of the most useful techniques for characterization of catalytic materials. It provides information about M-O bond arrangement and lattice defects. In the Raman experiment the intensity of scattered light is measured as a function of the frequency shift (Raman shift, cm^{-1}) of the photons. Due to interactions of light with different elementary excitations in solids, Raman spectroscopy is a powerful tool for the investigation of different solid state properties. That is why a Raman spectrum shows many

different features. In the project, Raman spectra were recorded with a Bruker senterra dispersive Raman microscope with laser excitation of wavelength of 532 nm, equipped with a confocal microscope and liquid-nitrogen cooled charge-coupled device (CCD) detector. The emission line at 532 nm from He-Cd laser (Melles Griot Laser) was focused on the sample under the microscope, with the diameter of the analysed spot being ~1 μm . The time of acquisition in both the cases was adjusted according to the intensity of the Raman scattering.

2.2.5 Transmission Electron Microscopy (TEM)

Transmission Electron Microscopy (TEM) offers increased resolution imaging, down to individual atoms, as well as ability of carrying out diffraction from Nano- sized volumes. TEM involves transmission of electrons through an ultra-thin specimen, interacting with the specimen as it passes through. An image is formed from the interaction of the transmitted electrons through the specimen. In a transmission electron microscope electrons are accelerated at high voltage (100- 1000 kV) to a velocity approaching the speed of light (.6-.9 c). The wavelength associated with these is five times smaller than that with light. A maximum thickness of 60 nm is required for TEM and HREM (High Resolution Electron Microscopy). Samples are deposited on 2/3 mm diameter carbon coated copper grids covered with a thin amorphous carbon film. In the project, the size and morphology of the nanoparticles were examined by using an FEI model TECNAI G 220 S-Twin TEM instrument.

2.2.6 X-ray Photoelectron Spectroscopy (XPS)

XPS utilizes photo-ionization and analysis of the kinetic energy distribution of the emitted photoelectrons to study the composition and electronic state of the surface region of a sample. X-ray Photoelectron Spectroscopy (XPS) involves use of soft x-rays i.e. the ones which have energy between 200-2000 eV. It is used to obtain information on chemical states from the variations in binding energies or chemical shifts of the sample. Here a photon is absorbed, by the sample, which causes ionization and emission of a core (inner shell) electron, as shown in fig. 3. The detector records the distribution of energy of these photoelectrons and gives a XPS spectra. An equation commonly used in XPS is

$$KE = h\nu - (BE + \phi_0)$$

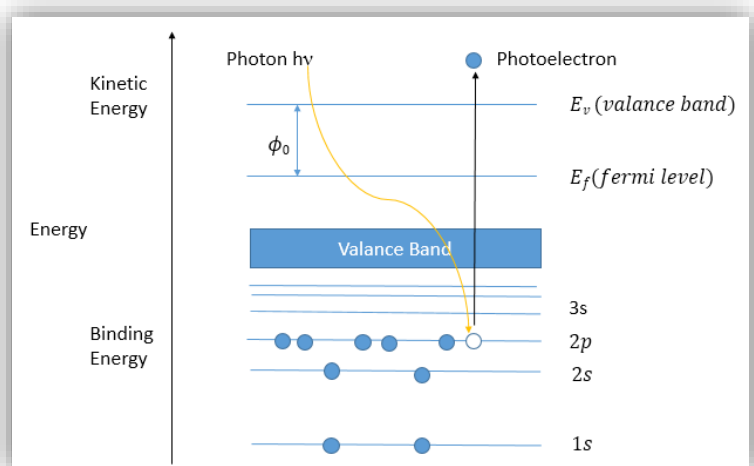


Figure 3: Electronic levels in an atom

XPS provides a quantitative analysis of the surface composition and hence it is also called ESCA (Electron Spectroscopy for Chemical Analysis). Two most common sources to be used are Mg (K_{α} radiation: 1253.6 eV) and Al (K_{α} radiation: 1486.6 eV). The exact binding energy of an electron depends not only on the element but also on the oxidation state of the atom and the local chemical and physical environment. The changes in these two parameters gives rise to chemical shifts which are recorded in the XPS spectra and hence this technique also distinguishes between the different oxidation states and chemical environments. In the present work, XPS data of the synthesized catalysts were recorded by an Axis Ultra instrument under ultra-high vacuum conditions and using a monochromatic Al (K_{α}) source (1486.6 eV).

3. Chapter 3

Decomposition of nitrous oxide

3.1 Introduction

Here we used cobalt oxide (Co_3O_4) as catalyst for N_2O decomposition. Also we prepared it using three different methods: hydrothermal, combustion and Coprecipitation and tested all three for nitrous oxide decomposition.

Later in order to improve its efficiency, we doped it with cerium oxide (CeO_2), prepared a series of catalysts, and then again tested it for N_2O decomposition.

3.2 Experimental section

3.2.1 Preparation of Co_3O_4

3.2.1.1. Combustion synthesis:

Cobalt nitrate ($\text{Co}(\text{NO}_3)_2 \cdot 6\text{H}_2\text{O}$) (taken as cobalt precursor) and citric acid ($\text{C}_6\text{H}_8\text{O}_7$) (cerium oxide precursor), purchased from Sigma, were dissolved in minimum amount of water and was sonicated for 15 min. Amount of the two reactants was determined by fuel: oxidant ratio, ϕ . It is a ratio of the total valency of oxidant to that of fuel. If $\phi = 1$ then the reaction is stoichiometric and the initial mixture doesn't require atmospheric oxygen for complete oxidation of fuel. $\phi > 1$ denotes oxidant rich (fuel lame) situation. $\phi < 1$ denotes fuel rich situation. The resultant solution was kept on hot plate so as to get a froth. This was then taken inside a preheated furnace maintained at 450°C for 15 min. The spongy solid so obtained was crushed to a fine powder and stored for further characterization and reactions. A sample prepared via combustion synthesis is shown in fig.4.



Figure 4: A sample prepared using combustion synthesis

3.2.1.2. Hydrothermal synthesis

Cobalt nitrate, cetyl trimethyl ammonium bromide (CTAB) and urea were dissolved in calculated amount of water and were stirred for 10 min. they were then transferred to a Teflon beaker and kept in a bomb, which was kept inside an oven at 160°C for 15 hrs. After the completion of reaction, contents were filtered and washed with water. They were then kept for calcination at 500°C for 12 hrs.

3.2.1.3. Coprecipitation synthesis

Cobalt nitrate was dissolved in optimum amount of water and was kept for stirring. To this, 2M sodium hydroxide solution was added drop wise to maintain pH around 11. Precipitate so obtained was left undisturbed for ageing overnight. Later it was filtered and washed with hot water. Solid so obtained was then calcined at 450°C for 12 hrs.

3.2.2. Preparation of Ce/Co catalysts using SCS

In order to improve the activity of cobalt oxide, cerium oxide was doped on it. A series of catalysts was prepared, by doping different amounts of cerium oxide, using combustion synthesis. Catalysts so prepared were labelled as xCeCo catalysts. Percentage of cerium oxide was varied from 10 to 100% $\{100 * \text{CeO}_2 / (\text{Co}_3\text{O}_4 + \text{CeO}_2) \%$ } so as to get xCeCo catalysts with different mole fractions of cerium oxide and cobalt oxide. Calculated amounts Co_3O_4 , ceric ammonium nitrate, CAN $(\text{NH}_4)_2\text{Ce}(\text{NO}_3)_6 \cdot 6\text{H}_2\text{O}$ (taken as cerium oxide precursor) and citric acid were dissolved in minimum amount of water. Contents were sonicated for 15 min. and later concentrated on a hot plate so as to get a froth. Later they were taken inside a preheated furnace maintained at 450°C for 15 min. Solid so obtained was crushed to a fine powder.

3.3 Results and discussion

For activity measurements, fixed amount of catalyst was taken in a quartz tube and placed in a temperature programmed furnace. Inlet of the tube was connected to N_2O cylinder (10 % N_2O in Argon) and products were analyzed by connecting the outlet to GC coupled with TCD

(Varian). A constant flow rate of 60 ml was maintained using MFCs'. All catalysts were initially placed at room temperature and then temperature was increased by 25°C till the final temperature was 450°C. A pictorial representation of experimental set up is shown in fig.5.

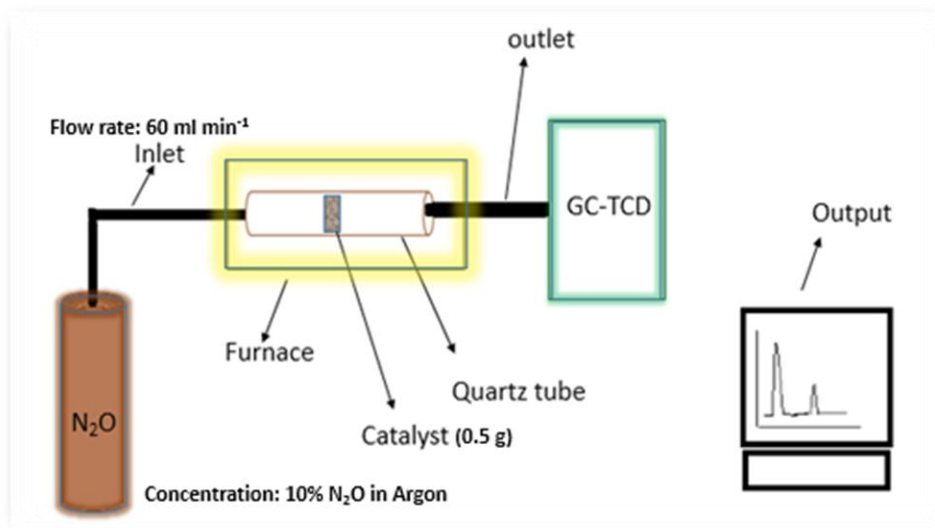


Figure 5: Activity measurement experimental setup

3.3.1 Characterization and activity measurements of Co_3O_4

3.3.1.1 P-XRD: Powder XRD patterns of Co_3O_4 prepared by combustion, Co-precipitation and Hydrothermal synthesis are shown in Fig.6. The patterns of Co_3O_4 shows characteristic peaks at (220), (311), (222), (400), (511) and (520) corresponding to cobalt oxide spinel structure. Most intense peak was corresponding to (311) plane and intensity of this plane for different samples was 36.85 for Coprecipitation, 36.85 for hydrothermal and 37.1 for combustion.

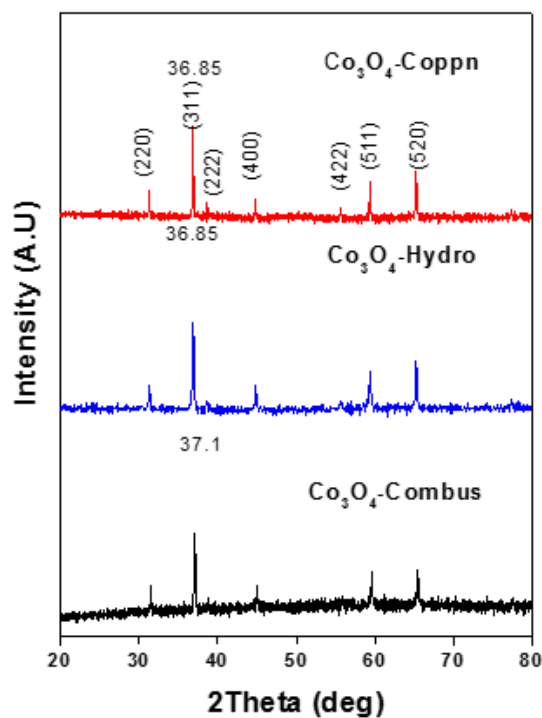


Figure 6: P-XRD patterns of Co_3O_4 prepared by different methods

3.3.1.2 Surface area determination: Surface areas of some of the synthesized catalysts, as determined using N_2 adsorption, BET analysis, are given in table 1.

Table 1: BET surface area of Co_3O_4 catalysts

Catalyst	Preparatory method	Surface area (m^2g^{-1})
Co_3O_4	Combustion	50
Co_3O_4	Co-precipitation	32
Co_3O_4	Hydrothermal	26

3.3.1.3. Raman Spectroscopy: Raman spectra of Co_3O_4 , prepared by different methods is shown in Fig.7.

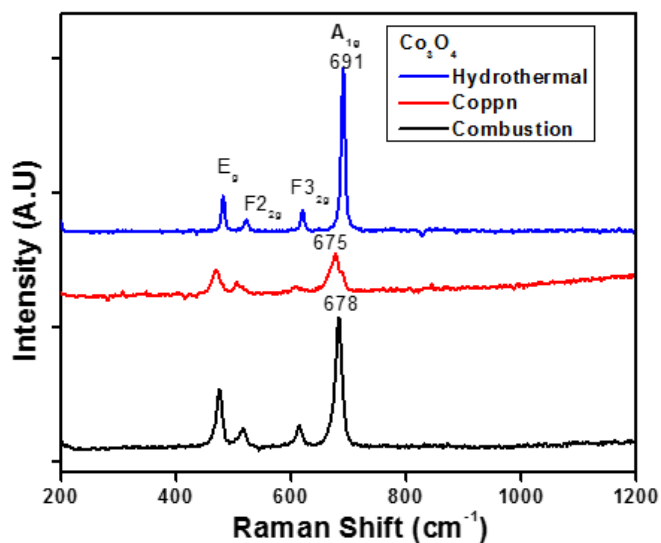


Figure 7: Raman spectra of Co_3O_4

Co_3O_4 belongs to the space group Oh, Fd3m and bulk Co_3O_4 has five major Raman active modes around 194, 482, 522, 618 and 691 cm^{-1} assigned to F_{2g} , E_g , F_{2g} , F_{2g} and A_{1g} respectively. The most intense A_{1g} peak (691 cm^{-1}) is assigned to the octahedral site CoO_6 symmetry and the E_g and F_{2g} peaks are together assigned to the tetrahedral site CoO_4 symmetry [27, 28].

3.3.1.4. UV Visible Spectroscopy: UV-Visible spectra of cobalt oxide catalysts is shown in Fig.8.

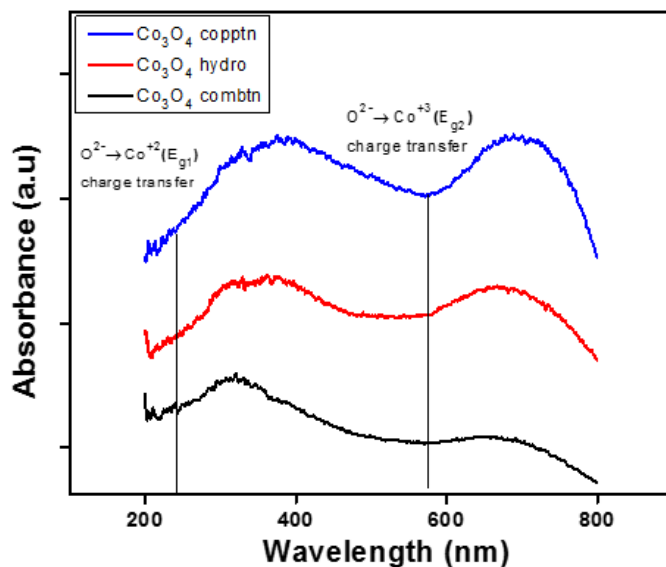


Figure 8: UV-Vis. Spectra of Co_3O_4

There are two bands corresponding to the two transitions occurring in the Co_3O_4 spinel. Both the transitions are ligand to metal charge transfer transitions. The lower wavelength band

corresponds to O^{-2} to Co^{+2} transition while the higher wavelength band corresponds to O^{-2} to Co^{+3} transition [29].

3.3.1.5. Temperature Programmed Reduction (TPR): TPR profile of cobalt oxide catalyst prepared by combustion synthesis is shown in Fig.9. It shows two peaks. According to the literature [30], the lower temperature peak, called the α peak (as shown in red color), corresponds to the reduction of Co^{+3} to Co^{+2} while the one at higher temperature, called β peak (shown in green) is for reduction of Co^{+2} to metallic cobalt, Co.

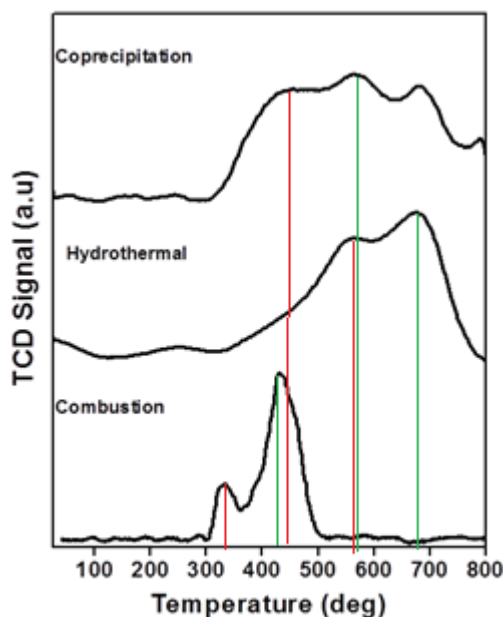


Figure 9: TPR of Co_3O_4

3.3.1.6. Activity measurement of Co_3O_4

Cobalt oxide, prepared by three different methods was tested for decomposition of nitrous oxide. The results are shown in Fig.10. Cobalt oxide prepared using combustion synthesis showed best activity among the three catalysts. This could be attributed to the fact that combustion synthesis has the ability to introduce more number of defects in the solid which tend to increase the catalytic activity of the material. Also it results in nanoparticles having large surface area, which is supported by BET analysis and Raman shift values. According to Raman spectra (Fig.7), Co_3O_4 sample prepared via hydrothermal synthesis has characteristic peaks at nearly the same position as those found in bulk Co_3O_4 however there occurs a deviation of about $13-16\text{ cm}^{-1}$ in case of Coprecipitation and combustion samples.

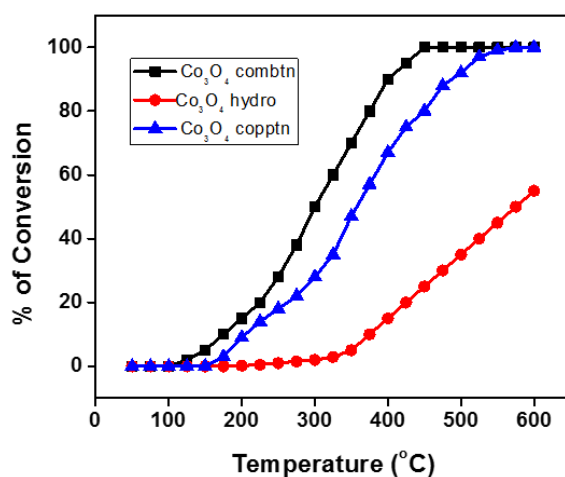


Figure 10: Decomposition of nitrous oxide by Co_3O_4

The reason for deviation is attributed to the optical phonon confinement in nanostructures, which can cause uncertainty in the phonon wave vectors and thus a downshift in the Raman peaks. This implies that nanoparticles are formed in case of combustion and Coprecipitation synthesis while hydrothermal generates bulk samples. [31]. Since the intensity of a particular peak, in Raman spectra, is an indication of the number of species responsible for that particular peak, it can be inferred from the above spectra that Co_3O_4 sample prepared from hydrothermal synthesis has more number of octahedral species (Co^{+3}) as compared to the other two samples. Also the sample prepared via combustion synthesis has more number of tetrahedral species (Co^{+2}). UV-Visible spectra of the Co_3O_4 samples support this proposal (Fig.8). There are two bands. A lower wavelength band corresponding to O^{-2} to Co^{+2} transition while the higher wavelength band for O^{-2} to Co^{+3} LMCT transition. It is clear from the spectra that there occurs a blue shift in both the bands as one moves from Coprecipitation to hydrothermal and combustion samples. This shift could be attributed to the quantum confinement of the nanoparticles which again indicates that combustion synthesis produces nanoparticles. Also from TPR profile (Fig.9), it is clear that Co_3O_4 prepared via combustion synthesis is an easily reducible species and hence shows better activity than the rest two. Hydrothermal sample has these peaks at highest temperature indicating its poor activity.

3.3.2 Characterization and activity measurements of Cerium oxide doped Co_3O_4 ($x\text{CeCo}$) catalysts

In order to improve the efficiency of the catalyst, cerium oxide was doped on cobalt oxide and these catalysts too were prepared using combustion synthesis. CeO_2 has been proposed as a component activating Co_3O_4 spinel for catalytic decomposition of N_2O . Xue et al. [24] have shown that the CeO_2 – Co_3O_4 oxide systems are significantly more active comparing to pure Co_3O_4 spinel and the activation effect of cerium is related to modifications of the redox properties of cobalt as well as preservation of the relatively high surface area of the catalysts (especially for the samples with low loading of cerium). The redox properties of CeO_2 – Co_3O_4 oxide systems and optimal composition of the catalysts were also described. Surface ceria oxygen is involved in oxidation of N_2O into the surface nitrogenated species. Decomposition of such species results in the formation of vacant sites on ceria, by oxygen depletion, and filling up such vacant sites by N_2O oxygen. Although this oxide system is very interesting for potential application in N_2O decomposition, the number of scientific reports related to this type of catalysts is rather limited. Up till now, the CeO_2 – Co_3O_4 catalysts for N_2O decomposition were synthesized by co-precipitation (with K_2CO_3 or KOH as precipitants), impregnation, citrate and thermal (thermal decomposition of mixture of $\text{Ce}(\text{NO}_3)_3$ and $\text{Co}(\text{NO}_3)_2$) methods. It was shown that method used for the synthesis of CeO_2 – Co_3O_4 oxide systems significantly differentiates their catalytic performance. Therefore, in this work, we applied another way for synthesis of CeO_2 – Co_3O_4 oxide system. Solution combustion method, guaranteeing the formation of nanocrystalline oxide materials, was used for the synthesis of two series of the samples, which were tested in the role of the catalysts for N_2O decomposition. Amount of cerium oxide was increased from 10 to 90 weight percent so as to have $x\text{CeCo}$ catalysts where x varied from 10 to 90 %. These catalysts too were characterized using XRD, BET, UV, Raman and TPR. The results are discussed in the following section.

3.3.2.1 P-XRD: Powder- XRD patterns of $x\text{CeCo}$ catalysts, prepared via combustion synthesis are shown in fig.11. All the reflections of pure cobalt oxide and pure cerium belong to cobalt spinel structure and fluorite oxide-type structure respectively. No other phase was detected on these $x\text{CeCo}$ catalysts except from these two phases.

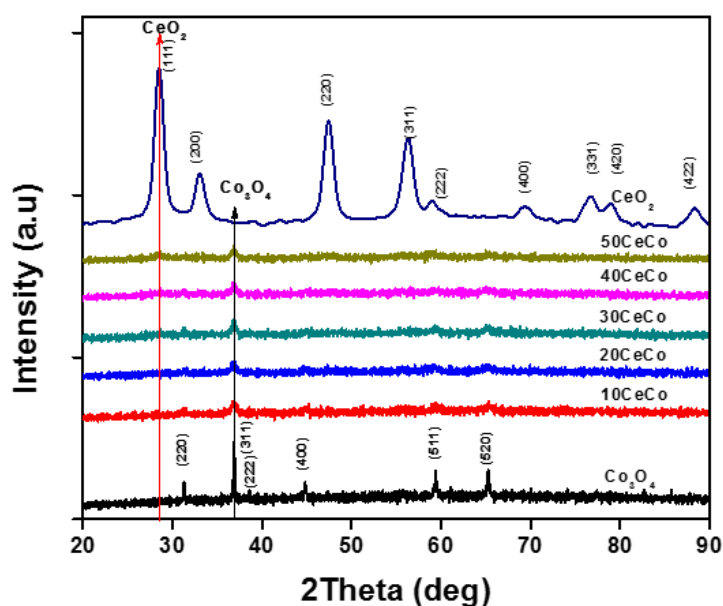


Figure 11: XRD pattern of xCeCo catalysts

The P-XRD patterns show prominent peaks at 2θ values of 19.1, 31.4, 36.8, 38.6, 44.9, 56.3, 59.3 and 65.4 which are indexed respectively as (111), (220), (311), (222), (400), (422), (511) and (440) planes of FCC type Co_3O_4 with space group of $\text{Fd}\bar{3}\text{m}$ (227). The diffraction lines corresponding to the ceria phase started appearing after 40% ceria content i.e. 40CeCo onwards. The intensity of Co_3O_4 signals increases with the cobalt content. The CeO_2 lattice constant in the undoped ceria catalyst is 5.14 Å. The lattice constant of Co_3O_4 in 10 to 50CeCo is equals 8.18 Å (Table 2).

Table 2: lattice parameters, surface area and particle diameter of xCeCo catalysts

Catalyst	Surface area ($\text{m}^2 \text{g}^{-1}$)	Lattice parameter (Å)		XRD Particle diameter (nm)	
		CeO_2	Co_3O_4	CeO_2	Co_3O_4
Co_3O_4	50	-	8.1801	-	8
10CeCo	65	5.09	8.1800	15 (10 nm from TEM)	8 (4 nm from TEM)
20CeCo	70	5.10	8.1800	-	9
30CeCo	72	5.11	8.1800	-	10
40CeCo	75	5.12	8.1800	-	12
50CeCo	78	5.14	8.1800	-	15
CeO_2	80	5.14	-	18	-

3.3.2.2 Determination of surface area (BET analysis): The specific surface area of xCeCo catalysts are given in table 2 above. In accordance with the XRD results, the specific surface area of xCeCo catalyst increased from 50 (for pure Co_3O_4) to $78 \text{ m}^2\text{g}^{-1}$ with the increase of ceria content. Surface area of pure CeO_2 had the maximum surface area among these catalysts. The above results indicate that an appropriate amount of Co in xCeCo could help to stabilize the catalyst structure and obtain a larger surface area in these catalysts.

3.3.2.3 TEM: Figure 12 shows typical TEM images taken over the bare CeO_2 support (a) and 10CeCo catalysts (b). The areas highlighted by the black circles indicate Co_3O_4 particles. Overall, Co_3O_4 particles are well dispersed throughout the entire CeO_2 particle surfaces examined. The cobalt oxide particles are easily discriminated from the CeO_2 particles, due to their distinct morphological difference. The CeO_2 support has a characteristic rectangular shape as seen in the TEM images taken before Co loading, whereas, the Co_3O_4 particles formed after doping of CeO_2 to Co_3O_4 are mostly round. Moreover, the Co_3O_4 and CeO_2 phase identifications have also been confirmed through characteristic lattice structure analysis at high resolution with lattice fringe spacing of 0.24 nm for Co_3O_4 ($[3\ 1\ 1]$) and 0.27 nm ($[1\ 0\ 0]$) for CeO_2 , respectively. Lattice parameter values re-establish the fact that the only phases present in the xCeCo catalysts are the individual phases and not mixed oxides.

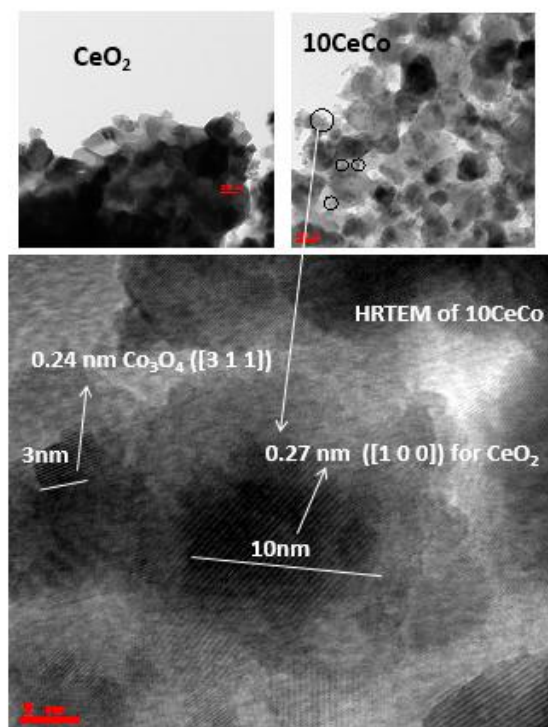


Figure 12: TEM image of (a) CeO_2 and (b) 10CeCo catalyst

3.3.2.4 XPS: XPS spectrum of Co and Ce in Ce₁₀Co is shown in fig.13. The spectra shows Co 2p_{1/2} and 2p_{3/2} peaks at 795 eV and 780 eV respectively. Some satellite peaks are also observed, indicating the presence of both +2 and +3 oxidation states. The XPS spectra of Ce 3d shows number of peaks in 3d_{5/2} and 3d_{3/2} region. These peaks are at 882, 889, 898, 900.7, 907.3 and 916 eV. CeO₂ XPS spectra is difficult to interpret because of the possibility of +3 oxidation state. However complete overlap of 3d region clarifies this discrepancy. Hence the only species present in CeO₂ is Ce⁺⁴. Presence of characteristic peaks in the spectra supports the proposal that the only phases that are formed in xCeCo catalysts are the individual phases and no mixed oxides are produced [32].

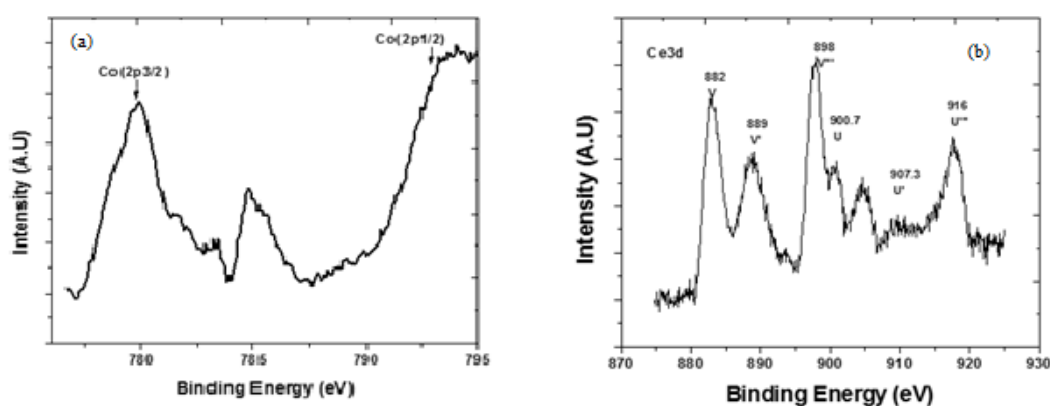


Figure 13: Core level XPS spectra of 10CeCo (a): Co (2p), (b): Ce (3d)

3.3.2.5. Raman spectroscopy: Raman spectra of xCeCo samples prepared by combustion synthesis is shown in Fig.14. Cerium oxide is much more Raman active than cobalt oxide [32]. Cerium oxide shows only one characteristic Raman peak at 464 cm⁻¹. As the content of cerium oxide increases, the 484 cm⁻¹ peak of cobalt oxide gets masked by cerium oxide peak. Also the intensity of both the modes (A_{1g} and F_{2g}) decreases with the increase in cerium oxide content. This indicates that there is replacement of some Co^{+2/+3} species by cerium upon doping. There occurs a considerable broadening of peaks too. It might be due to change in the composition of Co₃O₄ oxide. When a perfectly octahedral metal oxide undergoes displacement by other metal ions to generate a mixed metal oxide, its Raman spectra gets broadened due to interactions between different metals.

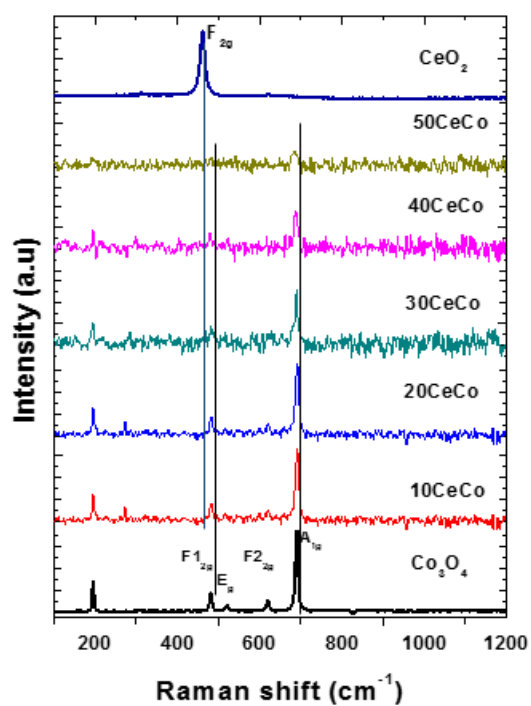


Figure 14: Raman spectra of xCeCo catalysts

3.3.2.6. UV-Visible spectroscopy: the UV-visible spectra of xCeCo catalysts is shown in fig.15.

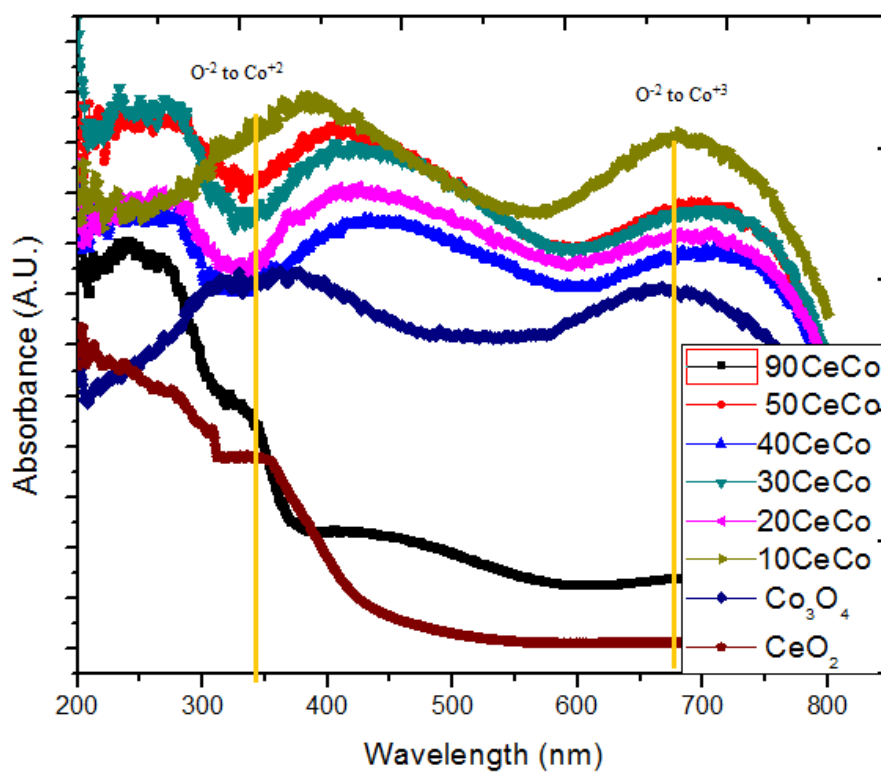


Figure 15: UV-Visible spectra of xCeCo catalysts

The lower wavelength band corresponding to O^{2-} to Co^{+2} LMCT transitions while the higher wavelength band corresponding to O^{2-} to Co^{+3} remains almost unchanged. This implies that cerium oxide doping interacts with Co^{+2} more than Co^{+3} and stabilizes it more. Thereby decreasing the energy separation between O^{2-} and Co^{+2} levels which facilitates such transition. Also the intensity of the first band increases as compared to other band, as cerium oxide content increases. This indicates that cerium oxide introduction makes the charge transfer process more feasible as a result of increased interactions. TPR data supports this observation, as discussed in next section.

3.3.2.7. **TPR:** The TPR profile of $xCeCo$ catalysts is shown in fig.16. Cerium oxide exhibits 2 peaks. The first peak is a low temperature peak which appears at about $500^{\circ}C$ which is assigned for the reduction of surface capped oxygen. While another high temperature peak at about $800^{\circ}C$ corresponds to the reduction of bulk oxygen [33].

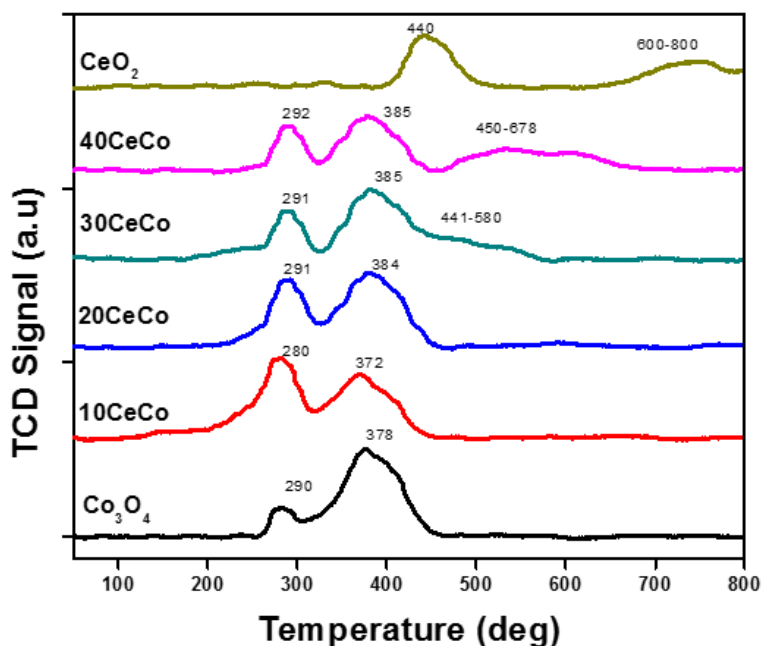


Figure 16: TPR profile of $xCeCo$ catalysts

Cobalt oxide shows its two characteristic reduction peaks, as explained in earlier sections. An observation to be made is regarding the intensity of the two peaks. The intensity of α peak increases while that of β peak decreases upon an increase in the content of cerium oxide. Moreover a considerable broadening of β peak occurs. The increased intensity implies that more Co^{+3} species are now undergoing reduction as compared to the Co^{+2} species. Also tailing can be explained by weak reducibility of cerium oxide. Thus presence of cerium oxide makes reduction of Co^{+2} difficult which could be attributed to the increased interactions between the two.

3.3.2.8. Activity measurement:

Under the same experimental conditions, described above, xCeCo catalysts were tested for nitrous oxide decomposition. As is clear from figure 17, addition of CeO₂ to Co₃O₄ obviously improves the catalytic activity of the catalyst. The promotion effect is strongly dependent on the molar ratio of Ce/Co. In the case of Co₃O₄, the reaction light-off temperature (50% N₂O conversion) is 300°C, and the complete conversion temperature is 450°C. Addition of small amounts of CeO₂ to Co₃O₄ increased the activity, so that, for the sample 20CeCo, the reaction reaches 50% conversion at 250°C and reaches 100% conversion at nearly 380°C.

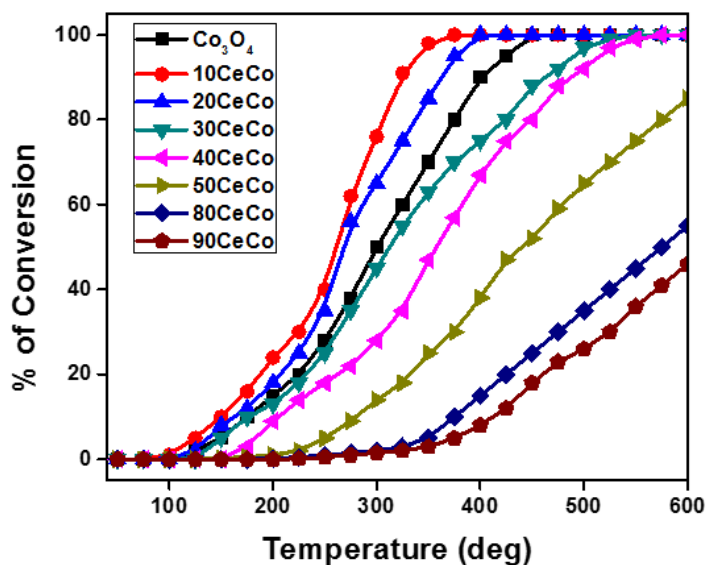


Figure 17: N₂O decomposition by xCeCo

With further increase of Ce, the promotion effect of CeO₂ on the catalytic activity was weakened. Pure CeO₂ was almost inactive for the decomposition of N₂O below 400°C (not shown in figure).

10CeCo catalyst shows the highest activity for the decomposition reaction in this series. 50% conversion was achieved at 230°C while 100% conversion was achieved at 350°C. From BET surface area it can be suggested that the increased surface area is a very important factor for the high catalytic activity of 10CeCo. In addition, the presence of appropriate amount of CeO₂ could minimize the crystallites of Co₃O₄, and thus improve its reduction behavior. When more CeO₂ was added, the promotion effect of CeO₂ on the reduction behavior of Co₃O₄ was weakened. In addition, available active site (Co²⁺) on the surface of the catalysts decreased because of the surface segregation of CeO₂. Therefore, the catalytic activity of xCeCo (x > 10 wt. %) decreased, even though they have larger surface area than 10CeCo.

It is clear from characterization data that cerium oxide interacts with Co⁺² more than Co⁺³. Moreover the activity of catalysts decreases as content of cerium oxide is increased beyond

20 mass %. Hence it can be proposed that Co^{+2} is the active site for reaction to occur. More cerium oxide means more interactions which in turn implies less availability of Co^{+2} for reaction. These interaction are favorable at low cerium oxide concentrations because it leads to better dispersion and stabilization of active species. However high concentrations might bind to these species more strongly thereby rendering them less available for reaction.

Activation energies (E_a) of the reaction over xCeCo catalysts were calculated according to the Arrhenius equation and results are shown in Fig.18.

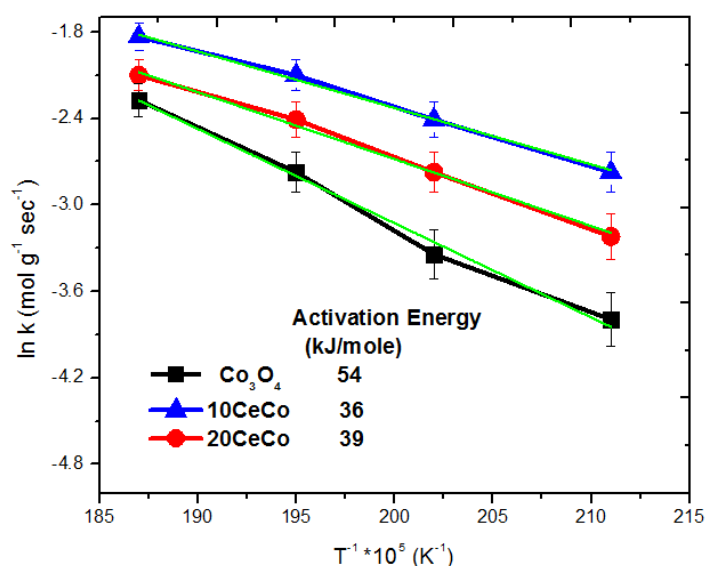


Figure 18: Activation energy calculations for Co_3O_4 , 10CeCo and 20CeCo

0.5g of catalyst was taken and kept inside quartz tube. N_2O was flushed through inlet at a flow rate of 60 ml min^{-1} . According to our results, the activation energies vary with the ceria loading and follow the order: Co_3O_4 (54 kJ mol^{-1}) < 20CeCo (39 kJ mol^{-1}) and 10CeCo (36 kJ mol^{-1}). 10CeCo sample is better than the other active catalysts. Comparison of these results with the TEM analysis, suggests that the change of surface morphology and the optimal ceria loading can increase both dispersion and surface area of catalyst and reduces the activation energies that can affect the rate of catalytic N_2O decomposition.

During our earlier studies, we tested few commercially available catalysts like $\text{Co}/\text{Al}_2\text{O}_3$, $\text{Rh}/\text{Al}_2\text{O}_3$ and $\text{Ir}/\text{Al}_2\text{O}_3$. However none of them showed appreciable activity for decomposition of nitrous oxide. Although literature provides sufficient data about the activity of Rh for nitrous oxide decomposition [5] but nature of support can drastically change the activity of a catalyst as was evident in our experiment.

3.4 Conclusions

Three different Co_3O_4 catalysts were prepared by solution combustion, hydrothermal and Coprecipitation methods. More importantly, contribution of each Co_3O_4 species in N_2O decomposition was evaluated. It was found that the Co_3O_4 catalyst by combustion method showed better activity of N_2O decomposition than rest of two methods.

A single step solution combustion method was employed to prepare a series of Ceria doped cobalt oxide catalysts so as to enhance the activity of Co_3O_4 . The resultant catalysts were characterized and evaluated for N_2O decomposition. Lattice oxygen is highly activated because of the Ce substitution and it plays a key role in decomposition of N_2O and influences the oxygen storage capacity and properties such as reducibility and reduction temperature. According to the results we got, it can be concluded that the optimum loading of ceria is 10wt. % (10CeCo). The 10CeCo sample exhibits highest surface area and best catalytic activity on N_2O decomposition ($T_{50} = 250^\circ\text{C}$) among these catalysts. We propose that the optimal ceria loading can increase both dispersion and surface area of catalyst and weaken the Co–O bond strength to promote the N_2O decomposition activity.

4. Chapter 4

Partial oxidation of methane using nitrous oxide

4.1 Introduction

Initial catalytic reactions for methane oxidation were based on the concept of activation of C-H bond. Of the most commonly used catalysts were molybdenum and vanadium based. First report of usage of molybdenum oxide, MoO₃ was published by Dowden and Walker [16]. Later Spencer exploited silica supported MoO₃ catalysts [17]. However soon it was realized that this is not a viable process and hence a new concept was developed. This involved a catalyst capable of transferring and stabilizing active oxidizing species. Some of the early works involved use of mixed metal oxides like Mo-V-Cr-Bi-Ox/SiO₂ [18]. Since this process is an oxidation process, several oxidizing agents have been tested like air [19], peroxide [20] etc. Nitrous oxide too has been exploited for the said reaction. One of the earliest report for this was by Lunsford and co-workers who used Mo/SiO₂ [21]. Later other catalysts like Ru/alumina [22], Co-Al/Au [23] etc.

4.2 Experimental section

4.2.1 Catalyst preparation:

10CeCo was giving best activity for N₂O decomposition and that catalyst was used in partial oxidation of methane. The catalyst was prepared using combustion synthesis as described in previous chapter.

4.2.2 Catalyst characterization

The catalyst was synthesized by following techniques P-XRD, UV-visible spectra and Raman spectroscopy, TPR, XPS and TEM. Results are described in previous chapter.

4.2.3. Activity measurements

0.5 g of catalyst was taken in a quartz tube and 30 ml each of N₂O (10% Ar) and CH₄ (10 %) were flushed in, through inlet. The furnace temperature was increased from room temperature to 550°C and the products were analyzed using GC-TCD.

4.3 Results and discussions

Under the given experimental conditions, decomposition of nitrous oxide was greater than methane. The conversion data of both the gases is shown in fig.19.

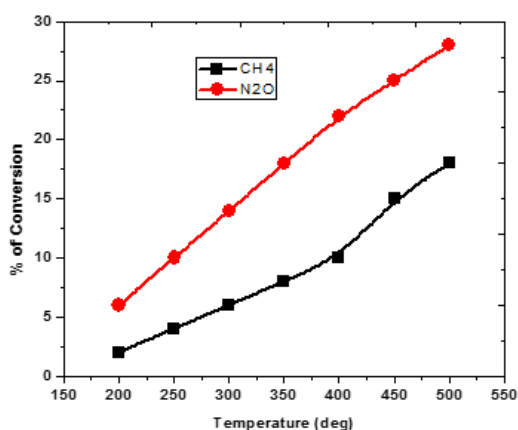


Figure 19: Conversion data for N₂O and CH₄

At 500°C, the maximum conversion for N₂O was nearly 30% while for CH₄, it was 15%. Apart from methanol, various other products were also formed upon partial oxidation of methane. Some of them were formaldehyde, carbon monoxide, carbon dioxide and hydrogen. Selectivity profile for all of them is shown in fig.20.

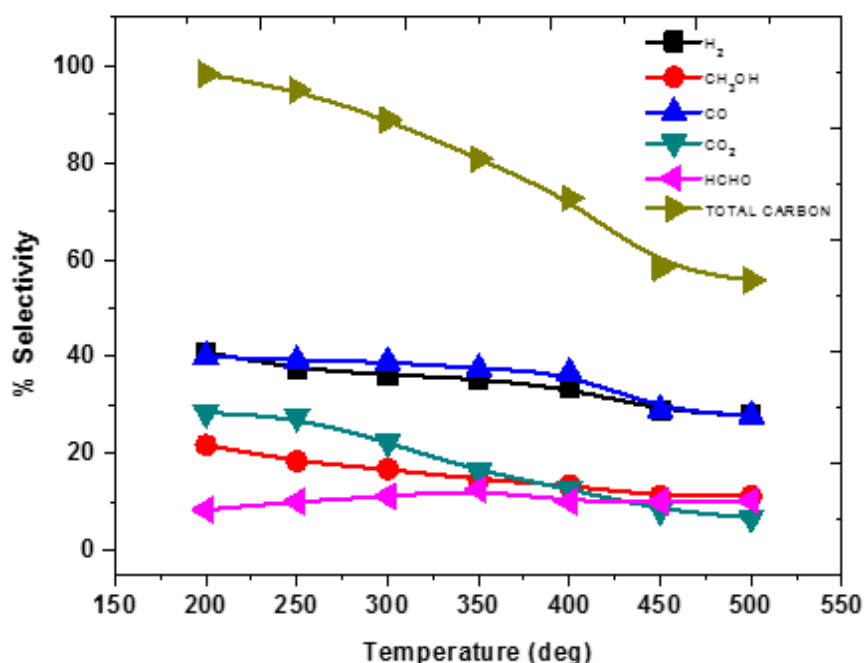


Figure 20: Selectivity profile of various products

The maximum selectivity towards various products is: H₂ 40%, methanol 20%, carbon monoxide 40%, carbon dioxide 30% and formaldehyde 15%. Selectivity towards methanol was found to decrease with increase in temperature. Similar case was observed for CO, CO₂ and H₂. However for formaldehyde, the selectivity was initially found to increase and later stabilized at higher temperature. With the increase in time, an appreciable decrease was observed in total carbon content. This indicates that at higher temperature, other unidentified compounds are also formed which decreases the selectivity towards the identified products. These compounds were determined qualitatively using GC-MS and were found to be higher hydrocarbons like acetylene, ethene etc. (no quantitative measurement of these compounds was done).

4.4 Conclusions

Partial oxidation of methane was done using 10CeCo catalyst prepared using combustion synthesis. Maximum conversion of methane and nitrous oxide was nearly 15 and 30%. Percentage selectivity towards all products is shown table 3.

Table 3: Selectivity towards different products upon partial oxidation of CH₄ using N₂O

Product	Percentage selectivity (at 500°C)
Methanol	15%
Formaldehyde	15%
Hydrogen	30%
Carbon monoxide	30%
Carbon dioxide	10%
Total carbon content	60%

Cerium oxide on cobalt oxide is known to be an effective oxygen stabilizer and this property is utilized in partial oxidation of methane using nitrous oxide. With the increase in temperature percentage conversion increases however selectivity towards methanol decreases.

There is great scope of further improvement of catalysts having better selectivity towards methanol.

5. References

1. A.R Ravishankara, John S Daniel et al. Nitrous Oxide (N₂O): The Dominant Ozone-Depleting Substance Emitted in the 21st Century. *Science*, (2009) 362.
2. Caillol Sylvain, Richter Renaud-de. Fighting global warming: the potential of photocatalysis against CO₂, CH₄, N₂O, CFCs, tropospheric O₃, BC and other major contributors to climate change. *Jphotochemrev* 12, (2011) 1-19.
3. F. Kapteijn, J. Rodriguez, J. A. Moulijn. Heterogeneous catalytic decomposition of nitrous oxide. *Appl. Catal. B* 9, (1996) 25-64.
4. G.I. Panov, A.S. Kharitonov, V.I. Sobolev Oxidative hydroxylation using dinitrogen monoxide: a possible route for organic synthesis over zeolites. *Appl.catal.A.* 98, (1993)1-20.
5. W. M. Kalback , C. M. Sliepcevich. Kinetics of Decomposition of Nitrous Oxide. *Ind.Eng.Chem.Fundam* 17, (1978) 165.
6. M. Hussain, D. Fino, N. Russo. N₂O decomposition by mesoporous silica supported Rh catalysts. *J. Hazard. Mater.* 211, (2012) 255-265.
7. H. Yoshida, T. Tsuruta, Y. Yazawa, T. Hattori. Support effect on oxidation resistance of precious metal catalysts as examined by N₂O decomposition. *Appl. Catal., A* 325, (2007) 50-56.
8. H. Zhou, Z. Huang, C Sun, F Qin, D Xiong. Catalytic decomposition of N₂O over Cu_xCe_{1-x}O_y mixed oxides. *Appl. Catal. B* 125, (2012) 492-498.
9. H. Gandhi, M. Shelef, K. Otto. The oxidation of CO by O₂ and by NO on supported chromium oxide and other metal oxide catalysts. *J.Catal.* 12, (1968) 361-375.
10. X. Xie, Y. Li, Z. Liu, M. Haruta, W. Shen. Low-temperature oxidation of CO catalyzed by Co₃O₄ nanorods. *Nature* 458, (2009) 746-749.
11. N. Bahlawane et al. Kinetics of methane combustion over CVD-made cobalt oxide Catalysts. *Appl. Catal. B* 67, (2006) 168-176.
12. K. Schmidt, K. Krawczyk. The properties of cobalt oxide catalyst for ammonia oxidation *Appl. Catal., A* 175, (1998) 147-157.

13. E. Wilczowska et al. Direct nitrous oxide decomposition with a cobalt oxide catalyst Appl. Catal., A 389, (2013) 165-172.
14. Zhe DOU, Ming FENG, XU Xiu-feng. Catalytic decomposition of N₂O over Au/Co₃O₄ and Au/ZnCo₂O₄ catalysts. J Fuel Chem Technol 41(10), (2013) 1234-1240.
15. Zhang Qijian, He Dehua, Zhu Qiming. Partial Oxidation of Methane to Formaldehyde over Superfine Mo/ZrO₂ Catalysts. J. Nat. Gas Chem. 12(2), (2003).
16. Dowden D A, Walker G T, U K 1 244 001, 1971.
17. N. D. Spencer, C J. Pereira. Partial oxidation of CH₄ to HCHO over a MoO₃-SiO₂ catalyst: A kinetic study. AIChE J 33(11), (1987) 1808.
18. Z. S. Han, W. Pan, W. X. Pan et al. Preparation and effect of Mo-V-Cr-Bi-Si oxide catalysts on controlled oxidation of methane to methanol and formaldehyde. Korea J Chem Eng 15(5), (1998) 1.
19. N. R. Hunter, H. D. Gesser, L. A. Morton, P. S. Yarlogadda. Methanol formation at high pressure by the catalyzed oxidation of natural gas and by the sensitized oxidation of methane. Appl. Catal., A 57, (1990) 45.
20. A Rahim, M Hasbi, MM Forde, RL Jenkins. Oxidation of Methane to Methanol with Hydrogen Peroxide Using Supported Gold–Palladium Alloy Nanoparticles. Angew. 125, (2013) 1318-1322.
21. R.S. Liu, M. Iwamoto, J. H. Lunsford. Partial oxidation of methane by nitrous oxide over molybdenum oxide supported on silica. J. Chem. Soc. Chem. Commun, 78-79 (1982).
22. P. Reddy, Nayeem Pasha, Chalapathi Rao, N. Lingaiah. Direct decomposition of nitrous oxide over Ru/Al₂O₃ catalysts prepared by deposition–precipitation method Catal.comm. 8, (2007) 1406-1410.
23. XU Xiao-ling, XU Xiu-feng, Zhang Guo-tao, NIU Xian-jun, Preparation of Co-Al mixed oxide-supported gold catalysts and their catalytic activity for N₂O decomposition. J Fuel Chem Technol 37(5), (2009) 595-600.
24. L. Xue, C. Zhang, H. He. Catalytic decomposition of N₂O over CeO₂ promoted Co₃O₄ spinel catalyst. Appl. Catal., B 75, (2007) 167-174.
25. K. Asano, C. Ohnishi, S. Iwamoto. Potassium-doped Co₃O₄ catalyst for direct decomposition of N₂O. Appl. Catal., B 78, (2008) 242-249.
26. Maximilian Lackner, Franz Winter, Avinash K. Agarwal. Handbook of Combustion Synthesis (Vol. 5) John Wiley & Sons, 2010.

27. Na Chan Woong, Hyung-Sik Woo a et al., Controlled transformation of ZnO nanobelts into CoO/Co₃O₄ nanowires CrystEngComm. 14, (2012) 3737-37.
28. Jin Seog Gwag† and Youngku Sohn, Interfacial Natures and Controlling Morphology of Co Oxide Nanocrystal Structures by Adding Spectator Ni Ions Bull. Korean Chem. Soc 33, No. 2, (2012) 505.
29. Nasser A. M Barakat, Myung Seob Khil, Faheem A Sheikh. Synthesis and Optical Properties of Two Cobalt Oxides (CoO and Co₃O₄) Nanofibers produced by Electrospinning Process. J. Phys. Chem. C 112, (2008) 12225–12233.
30. Jin-bing Lia; Zhi-quan Jiangb; Kun Qianb; Wei-xin Huang, Effect of Calcination Temperature on Surface Oxygen Vacancies and Catalytic Performance Towards CO Oxidation of Co₃O₄ Nanoparticles Supported on SiO₂ Chin. J. Chem. Phys. 25, No. 1, (2012) 103-109.
31. Farhadi Saeid, Pourzare Kolsoum et al. Simple preparation of ferromagnetic Co₃O₄ nanoparticles by thermal dissociation of the [Co^{II}(NH₃)₆](NO₃)₂ complex at low temperature J Nanostructure Chem 3, (2013) 16.
32. H. Song, U. Ozkan. The role of impregnation medium on the activity of ceria-supported cobalt catalysts for ethanol steam reforming. J. Mol. Catal. A: Chem. 318, (2010) 21-29.
33. Boaro Marta, Vicario Michela et al., The use of temperature-programmed and dynamic/transient methods in catalysis: characterization of ceria-based, model three-way catalysts. Catal. Today 77, (2003) 407–417.